An ion mobility mass spectrometer coupled with a cryogenic ion trap for recording electronic spectra of charged, isomer-selected clusters

Jack Buntine, Eduardo Carrascosa, James Bull, Ugo Jacovella, Mariah Cotter, Patrick Watkins, Chang Liu, Michael Scholz, Brian Adamson, Samuel Marlton, et al.

An ion mobility mass spectrometer coupled with a cryogenic ion trap for recording electronic spectra of charged, isomer-selected clusters

Jack T. Buntine, Eduardo Carrascosa,[a] James N. Bull,[b] Ugo Jacovella,[c] Mariah I. Cotter, Patrick Watkins, Chang Liu, Michael S. Scholz,[d] Brian D. Adamson, Samuel J. P. Marlton, and Evan J. Bieske[e]
School of Chemistry, The University of Melbourne, Victoria, Australia 3010

(Dated: 27 February 2022)

Infrared and electronic spectra are indispensable for understanding the structural and energetic properties of charged molecules and clusters in the gas phase. However, the presence of isomers can potentially complicate the interpretation of spectra, even if the target molecules or clusters are mass-selected beforehand. Here we describe an instrument for spectroscopically characterising charged molecular clusters that have been selected according to both their isomeric form and their mass-to-charge ratio. Cluster ions generated by laser ablation of a solid sample are selected according to their collision cross section with helium buffer gas using a drift tube ion mobility spectrometer, and their mass-to-charge ratio using a quadrupole mass filter. The mobility- and mass-selected target ions are introduced into a cryogenically-cooled, three-dimensional quadrupole ion trap where they are thermalized through inelastic collisions with an inert buffer gas (He or He/N_2 mixture). Spectra of the molecular ions are obtained by tagging them with inert atoms or molecules (Ne, N_2), which are dislodged following resonant excitation of an electronic transition, or by photodissociating the cluster itself following absorption of one or more photons. An electronic spectrum is generated by monitoring the charged photofragment yield as a function of wavelength. The capacity of the instrument is illustrated with resonance-enhanced photodissociation action spectra of carbon clusters (C_n^+) and polyacetylene cations ($HC_{2n}H^+$) that have been selected according to mass-to-charge ratio and collision cross section with He buffer gas, and of mass-selected Au_2^+ and Au_2Ag^+ clusters.

I. INTRODUCTION

Infrared and electronic spectra provide important structural and energetic information on charged molecules and clusters. However, obtaining infrared and electronic spectra of molecular ions in the gas phase is a challenging enterprise due to low ion densities and the potential presence of different molecular species that absorb across the same spectral range. A successful strategy for confronting these obstacles involves mass selection of the target molecular ions followed by resonance enhanced photodissociation (REPD) of the ions, or of the ions tagged by weakly bound atoms or molecules (typically He, Ne, Ar or N_2), and detection of the photofragments.[1–23] The advantages are that mass selection reduces ambiguity regarding the identity of the absorbing species, and that the photofragment ions can be detected with high efficiency, conferring exceptional sensitivity. The approach, which works particularly well for molecular ions cooled in a supersonic expansion or in an ion trap, has been used to obtain infrared and electronic spectra for a vast array of charged molecules using light from tunable benchtop lasers and optical parametric oscillators, and free electron lasers. Other forms of action spectroscopy, including laser induced reaction[20] and laser suppression of clustering,[24] which also possess the advantages of mass-selectivity and high sensitivity, have also been deployed to probe infrared and electronic transitions of molecular ions.

Notwithstanding the advantage of mass-selection prior to spectroscopic interrogation, ambiguities remain when the target ions exist as two or more isomers with distinct infrared or electronic spectra. One method of distinguishing spectral features associated with different isomers is through hole-burning spectroscopy, whereby a fixed wavelength laser beam (IR, visible or UV) is used to deplete one isomer's population with a second laser beam tuned to probe the remaining isomer(s).[8–15] Although powerful, this approach requires several tunable lasers and becomes complicated if more than two isomers are present. Isomers of charged molecules, including $C_3H_3^+$ and protonated phenol, have also been distinguished by the manner in which they establish non-covalent bonds with tag atoms or molecules, and the infrared spectra of the tagged species.[25,26] An alternative isomer-selective strategy involves preselecting the target isomers according to their collision cross sections (CCS) with an inert buffer gas using some form of ion mobility spectrometer (IMS) before mass selection and spectroscopic interrogation. This IMS-MS approach has

[a] Bruker Daltonics GmbH & Co. KG, Fahrenheitstrasse 4, 28359 Bremen, Germany
[b] School of Chemistry, Norwich Research Park, University of East Anglia, Norwich NR4 7TJ, United Kingdom
[c] Université Paris-Saclay, CNRS, Institut des Sciences Moléculaires d'Orsay, 91405 Orsay, France.
[d] Department of Chemistry, University College London, London WC1H 0AJ, United Kingdom
[e] Electronic mail: evanjb@unimelb.edu.au

been implemented using either a drift tube ion mobility spectrometer,[27–29] field asymmetric ion mobility spectrometer (FAIMS),[30–33] differential mobility spectrometer (DMS),[34,35] or variants of traveling wave ion mobility spectrometers (TW IMS).[36,37] Instruments have also been developed in which photoisomerization or photodetachment of selected isomers were measured by photoexciting the target molecular ion between two ion-mobility stages.[38,39] Other instruments have been developed in which carbon cluster anions[40] or biomolecule anions[41] were mobility-selected prior to photoelectron spectroscopy.

In this paper we describe a new tandem ion mobility mass spectrometer combined with a cryogenically cooled ion trap (IMS-MS-cryo) that is suitable for spectroscopically interrogating charged clusters that are created through laser ablation of a solid sample, and which may exist as several different isomers. The cluster ions are selected according to their drift mobility in He buffer gas and their mass-to-charge ratio before being trapped and exposed to tunable light in a cryogenically cooled ion trap, with detection of charged photofragments separated in a time-of-flight-mass spectrometer. The requirement for an isomer-selective spectroscopic approach for charged clusters generated through laser ablation is apparent from previous ion mobility studies. For example, C_n^+ clusters formed by laser ablating graphite have been found to exist as linear isomers for n=3–10, monocycles for $n\geq$7, bicycles for $n\geq$21 and fullerenes for $n\geq$30, with the coexistence of different isomers over extended size ranges.[42] Corresponding studies have discovered coexisting isomers for many other charged clusters generated through laser ablation, including, C_n^-,[43] $Si_n^{+/-}$,[44,45] Ag_n^+,[46] $Au_n^{\pm}$,[47,48] $Ag_mAu_n^+$,[49] $Nb_mO_n^{\pm}$,[50] and $Fe_nO_n^+$ and $Fe_nO_{n+1}^+$ clusters.[51] Obtaining isomer-selective infrared and electronic spectra of these clusters is desirable because of their potential applications in materials science, and in some cases their possible presence in interstellar space.

The IMS-MS-cryo apparatus described in this paper is similar in concept to instruments developed by Rizzo and coworkers in which ions are preselected according to their collision cross sections and mass-to-charge ratio prior to being trapped and probed with tunable laser radiation in a cryogenic ion trap.[29–31,36,37] However, these instruments have been developed primarily for characterizing charged biomolecules generated with an electrospray ionization source rather than charged clusters generated through laser ablation of a solid sample. The IMS-MS-cryo instrument also has aspects common to the instrument developed by Campbell and coworkers for spectroscopically probing carbon clusters generated using laser ablation, but which does not feature an ion mobility stage.[52]

In the remainder of the paper we first provide an overview of the arrangement for forming, selecting and spectroscopically probing charged clusters, and continue by describing the IMS-MS-cryo instrument in detail. Next, we illustrate the instrument's performance by presenting ion mobility data and electronic spectra for C_n^+ clusters and polyacetylene cations ($HC_{2n}H^+$), showing that the clusters can be selected and probed according to their mass-to-charge ratio and their collision cross section. As further examples, we present electronic spectra of the Au_2^+ dimer and Au_2Ag^+ trimer, demonstrating the instrument's capacity for spectroscopically interrogating metal cluster cations.

II. OVERVIEW AND STRATEGY

The strategy for forming, selecting and spectroscopically probing cluster ions can be appreciated from the schematic illustration of the instrument in Figure 1(a). Although the figure refers to carbon cluster cations, the strategy is applicable to many other charged clusters. Ions generated by pulsed laser ablation of a solid sample (Region 1) are propelled through helium buffer gas by an electric field where they are separated spatially and temporally according to their collision cross sections with the buffer gas (Region 2). More extended ions have larger collision cross sections and traverse the drift tube more slowly than faster, more compact ions.

At the end of the ion mobility drift region the ions encounter an electrostatic ion gate that can be opened to transmit a packet of ions with a defined range of velocities (i.e. mobilities or collision cross sections). Following the ion gate, the ions are collected radially by an RF ion funnel before passing through an orifice into a hexapole ion guide (Region 3), and then through a quadrupole mass filter (Region 4) where they can be mass selected. From here, the ion beam can be deflected to an off-axis scintillator detector, which is connected to a multichannel scaler that can be used to generated a histogram of ion counts against arrival time, giving an arrival time distribution (ATD) for the ions.

Alternatively, the ion beam is allowed to continue through an octupole ion guide into a radio frequency quadrupole ion trap (QIT, Region 5), that can be cooled to a temperature of 4 K. The ions are collected and confined in the QIT where they are thermalized through inelastic collisions with an inert buffer gas (either He, Ne, 1% N_2 in He or 1 % N_2 in H_2). As they cool, weakly bound complexes form between the ions and buffer gas atoms or molecules. The clusters are overlapped with light from a tunable optical parametric oscillator (OPO), which, if tuned to an electronic transition, induces photodissociation. Following their irradiation, the ions are ejected from the QIT into a time-of-flight mass spectrometer (TOFMS, Region 6) and are detected by a dual microchannel plate (MCP) detector. Normally, the machine is run with a duty cycle of 2 Hz with alternate ion packets exposed to the OPO beam. Subtracting the light-off signal from the light-on signal affords the overall photore-

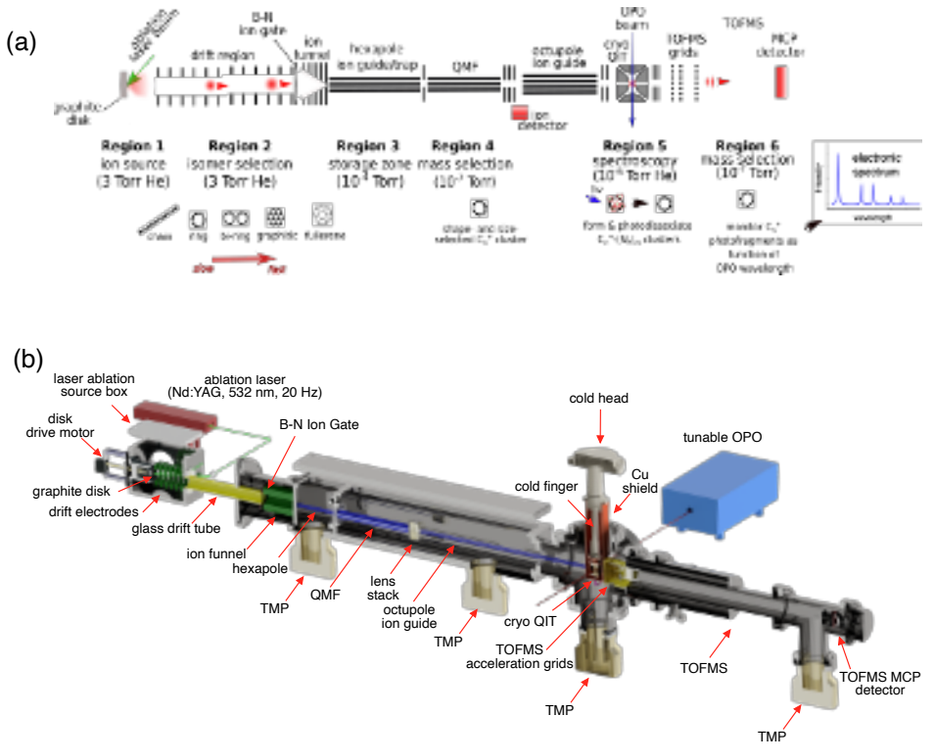

FIG. 1: (a) Schematic representation of the tandem IMS-MS-cryo instrument. Carbon cluster cations are used to illustrate the strategy, which is applicable to a broader range of charged clusters. Ions are formed through laser ablation of a sample (Region 1), separated in a drift tube ion mobility spectrometer filled with He buffer gas (Region 2), accumulated in a hexapole ion guide (Region 4), mass-selected in a quadrupole mass filter (region 4), introduced into a quadrupole ion trap where they are cooled and possibly tagged with N_2 molecules (Region 5), before being exposed to one or more pulses of tunable wavelength radiation. Ions are ejected from the trap and photofragments are separated according to their mass-to-charge ratio in a time-of-flight mass spectrometer (Region 6). (b) Sectioned three-dimensional view of the IMS-MS-cryo instrument. The off-axis scintillator detector between the QMF and octupole ion guide is not shown. TMP=turbomolecular pump, B-N=Bradbury-Nielsen, QMF=quadrupole mass filter, TOFMS=time-of-flight mass spectrometer.

sponse, which, when plotted against wavelength, gives the electronic action spectrum.

III. SEPARATION OF ISOMERS IN THE DRIFT TUBE ION MOBILITY SPECTROMETER

As described above, isomer separation is accomplished using a drift tube ion mobility spectrometer in which the ions are propelled by an electric field E through a buffer gas, attaining a velocity, v_d. In the low field regime,

$$v_d = KE, \tag{1}$$

where K, the mobility, is inversely proportional to the collision integral $[\Omega^{(1,1)}(T)]$ and is given by,[53]

$$K = \frac{3ze}{16N}\left(\frac{2\pi}{\mu k_B T}\right)^{\frac{1}{2}}\frac{1}{\Omega^{(1,1)}(T)} \tag{2}$$

Here, z is the charge state of the ion, e the elementary charge, k_B the Boltzmann constant, T the absolute temperature, and N the number density of the buffer gas molecules. The reduced mass μ is given by,

$$\mu = \frac{Mm}{M+m}, \tag{3}$$

where m is the mass of the ion and M is the mass of the buffer gas atoms. The collision integral $[\Omega^{(1,1)}(T)]$, which is related to the deflection angle of the colliding partners, averaged over velocity, collision orientation, and impact parameter, depends on the intermolecular potential energy surface for the interaction between the cluster ion and buffer gas atom or molecule, and is therefore sensitive to the cluster's isomeric structure.[53] For standardized reporting and comparison, the measured mobility is normally converted to the reduced mobility, K_0,

$$K_0 = K\frac{P}{760}\frac{273.2}{T} \tag{4}$$

where P is the pressure in Torr.

IV. INSTRUMENT CONSTRUCTION

A. Laser ablation ion source

The construction of the IMS-MS-cryo instrument can be appreciated from Figure 1(b). The first section of the machine is a laser ablation ion source connected to a drift tube ion mobility mass spectrometer and an ion funnel. This region is filled with He buffer gas (pressure ≈3 Torr) delivered at 0.2 SLM through a mass flow controller (Sevenstar, D08-1F) and pumped by a 12 m^3/hr rotary vane pump. Ions are produced by ablating the surface of a sample disk (ϕ=20 mm) using the frequency doubled output (532 nm) of a pulsed Nd:YAG laser (Quantel Ultra) operating at a repetition rate of 20 or 50 Hz with a pulse energy of ≈12 mJ and pulse duration of 5 ns. The laser beam is focussed on the sample disk surface using a 500 mm focal length lens. The sample disk is mounted on a hypocycloidal stage whose 0.1 Hz rotation is driven by a geared 12 V DC motor. The path of the ablation laser spot on the disk is a precessing ellipse, ensuring that material is removed evenly from the surface.

B. Ion mobility, ion storage and mass selection stages

The laser-ablated cluster ions immediately enter the drift region where they are propelled by an electric field through He buffer gas. The first stage of the drift region is 10 cm long and consists of 12 evenly spaced ring electrodes (inner diameter 40 mm), that are fabricated from printed circuit board (PCB), and which are coupled by 1 MΩ resistors. An electric field of 11 V/cm is established by applying electrical potentials of 550 V and 440 V to the first and the last electrodes, respectively. Following the ring electrode stack, the ions enter a 30 cm resistive glass tube with an inner diameter of 40 mm (Photonis),[54] which has a resistance of 33 MΩ. The entrance and exit ends of the tube are biased at 440 V and 170 V, respectively, generating a drift field of 9 V/cm. After exiting the glass drift tube, the ions encounter an electrostatic Bradbury-Nielsen ion gate consisting of interleaved tungsten wires,[55] that can be opened with an appropriate delay and width to transmit the desired isomer packet while blocking slower or faster isomers. Following the ion gate, the ions are gathered radially by an ion funnel (length=10 cm). The ion funnel comprises 45 ring electrodes fabricated on PCB with electrode inner diameters that decrease linearly from the entrance (ϕ=40 mm) to exit (ϕ=7 mm). The electrodes are connected by 1 MΩ resistors with appropriate potentials applied to the first and last electrodes to establish a drift field of 8 V/cm. The electrodes are capacitively coupled to the RF supply (drive amplitude 70 V_{pp}, frequency 808 kHz) .

After exiting the ion funnel, the ions pass through a 1 mm orifice in an electrode on a PCB board, that serves as a differential wall between the drift region and hexapole region, and enter an RF hexapole ion guide. The hexapole drive voltage is 80 V_{pp} with frequency 800 kHz. By changing its DC electrical potential, the hexapole can either be used as a simple ion guide or as a trap to store ions from several ablation laser pulses. The former operation mode is used for measuring ATDs of the laser-ablated clusters, whereas the latter mode is used if the ions are to be transferred to the QIT for spectroscopic interrogation. The hexapole chamber is pumped by two 240 L/s turbomolecular pumps, which maintain a pressure of ≈5×10^{-5} Torr during operation.

The ions pass from the hexapole through a 3 mm aperture in a plate electrode into the QMF, where they are mass selected. The chamber containing the QMF is evacuated by a 240 L/s turbomolecular pump and has an operating pressure of ≈2×10^{-6} Torr. Following mass-selection in the QMF, the ions can be deflected to an off-axis scintillator detector that is connected to a multichannel scaler (MCS, FAST ComTec, MCS-4), which can be used to record an arrival time distribution (ATD) of the ions. The IMS stage, when operating with He buffer gas, possesses a mobility resolution of ≈20, which is sufficient to distinguish carbon cluster chains, rings, bi-rings and fullerenes for clusters containing up to 70 carbon atoms. The resolution of the QMF can be adjusted to be ≤0.5 amu for clusters up to C_{60}^+, albeit with some sacrifice of transmission.

C. Cryogenically cooled quadrupole ion trap

For spectroscopic characterization, the ions are transferred by an octupole ion guide (drive voltage 28 V_{pp}, frequency 800 kHz) through three electrostatic lenses to the QIT (R.M. Jordan TOF Products, INC. C-1251). The arrangement for cooling the QIT follows the scheme described in ref. 56. The QIT is driven at a frequency of 1 MHz with typical amplitude of 500–900 V_{pp}. The original stainless steel electrodes of the QIT were replaced with oxygen-free copper electrodes to achieve better thermal conductivity, and were sputter coated with gold (thickness ≈150 nm) to reduce accumulation of surface charge. The QIT is cooled using a closed-cycle cryocooler unit (RDK-205E 4K, Sumitomo Heavy Industries, Ltd.). The trapped ions are vibrationally and rotationally relaxed through inelastic collisions with a buffer gas (either He, Ne, 1% N_2 in H_2, 1% N_2 in He) delivered through a pulsed solenoid valve (General Valves, Series 9) mounted on the chamber wall. The outlet of the pulsed valve is connected by a teflon tube to a section of copper tube mounted on the copper cryotrap shield where the buffer gas is pre-cooled before passing through a thin delrin tube inserted into a small hole in the QIT ring electrode. The pulsed valve is normally opened for ≈200 μs at the beginning of the trapping cycle, ≈20 ms before

the ions are released from the hexapole ion guide. The chamber containing the QIT is evacuated by a 900 L/s turbomolecular pump and has an operational pressure of $\approx 10^{-6}$ Torr.

The QIT temperature can be adjusted by passing current through resistors attached to the QIT mount. The temperature is monitored using a Lakeshore DT-670 silicon diode attached to the mount. A QIT temperature of ≈25 K worked well for generating N_2-tagged clusters using a gas mixture of either 1% N_2 in He or 1% N_2 in H_2. Eventually, after ≈8 hours, the QIT electrodes are normally coated with a layer of solid N_2, affecting operation and necessitating heating of the trap to 80 K, before re-cooling and resuming operation.

D. Time-of-flight mass spectrometer and ion detection

For mass analysis and detection, the molecular ions are ejected from the QIT into the acceleration region of a 0.9 m linear time-of-flight mass spectrometer (TOFMS). The electrical potentials to the first and second acceleration grids of the TOFMS are supplied through two high-voltage switches (Behlke HTS 61-02) with the electrical potentials adjusted to achieve Wiley-McLaren space focussing. The ions are detected at the end of the flight tube by a tandem microchannel plate (MCP) assembly, the output of which is sent to a computer-based oscilloscope (Picoscope 5000). The TOFMS has a mass resolution of $m/\Delta m \approx 1000$, sufficient to distinguish neighbouring mass peaks for carbon clusters containing different numbers of ^{13}C atoms, at least up to C_{60}^+.

The ions are separated temporally and spatially according to their m/z over the short section between the QIT and the source region of the TOFMS – this section acts as a short TOFMS. The optimal delay between ejection of ions from the QIT and firing of the TOFMS acceleration grids depends on the ion mass, and is adjusted to maximize the ion signal recorded at the MCP detector of the TOFMS. Several digital delay generators (Quantum Composers 9400 Series) are used to synchronize the triggering of the ablation laser, ejection of ions from the hexapole trap, opening of the gas nozzle, firing of the photodissocation laser pulses, ejection of ions from the QIT, and switching of the TOFMS acceleration potentials.

E. Recording electronic spectra

Resonance enhanced photodissociation spectra are obtained by measuring the target cluster ion signal and photofragment ion signal as a function of the excitation wavelength. Usually, ions generated by laser ablation are stored in the hexapole and are released at a rate of 2 Hz through the QMF into the QIT. After 480 ms the ions are ejected from the QIT into the TOFMS for mass analysis. In the QIT, alternate ion packets are exposed to unfocussed light from a tunable optical parametric oscillator (EKSPLA NT342B, 5 cm^{-1} bandwidth, 5 ns pulse width). Resonant photoexcitation causes destruction of the parent clusters and corresponding formation of photofragment ions. Normally, the intensity of the OPO beam and the number of OPO shots delivered to the ion packet are adjusted to ensure that ≤5% of the ions are photodissociated when the light is tuned to the most intense transition. Typically, to accomplish this, the trapped ions are exposed to only a single pulse of light from the OPO that was selected using a mechanical shutter. However, for weaker transitions or in spectral regions where the OPO output is low, the ions are exposed to several light pulses. Under these conditions, the photofragment signal plotted against wavelength gives the REPD spectrum.

It should be emphasized that the REPD action spectrum represents a convolution of the cluster's absorption spectrum and a function describing the wavelength-dependent photodissociation yield. The difference between the absorption spectrum and the REPD spectrum can be minimal if the target cluster is tagged by a weakly bound atom or molecule (e.g. He, Ne, Ar or N_2), or if the photon energy exceeds the dissociation energy and there is a viable path to dissociation that is more efficient than competing deactivation processes. In contrast, there can be substantial differences between the REPD spectrum and the absorption spectrum if the accessed vibrational or electronic state lies below the dissociation threshold, such that only clusters already possessing vibrational energy or which absorb several photons are able to photodissociate.

V. INSTRUMENT PERFORMANCE

A. IMS-MS Performance - Arrival Time Distributions for C_n^+ Clusters

The performance of the IMS-MS section of the instrument can be exemplified with arrival time distributions for carbon cluster cations formed by laser ablation of a graphite disk. To do this, the machine is operated with the ions passing directly through the hexapole ion guide and being detected by the off-axis detector situated after the QMF (see Figures 1(a)). The isomeric distribution of C_n^+ clusters with n=10–40 is illustrated in Figure 2, where the ion signal is plotted as a function of arrival time and mass-to-charge ratio. The data are consistent with previous ion mobility measurements from ref. 42, albeit with slightly better resolution of the ATD peaks. Peaks associated with monocyclic carbon clusters are apparent for $n \geq 10$, bicyclic clusters for $n \geq 21$ and fullerenes for $n \geq 32$. Importantly, for some size ranges there is a coexistence of two or more isomers. For example, C_{36}^+ exists as monocyclic, bicyclic and fullerene isomers (see Figure 2). We

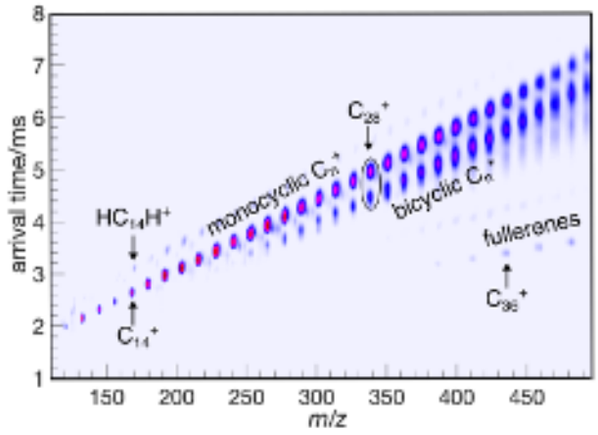

FIG. 2: Ion signal as a function of m/z and drift time for carbon cluster cations formed by laser ablation. Peaks are apparent for C_n^+, C_nH^+ and $C_nH_2^+$ ions.

TABLE I: Calculated and measured reduced mobilities (K_0) for monocyclic C_{2n}^+ clusters and $HC_{2n}H^+$ (n=5-8) clusters in He buffer gas (units $cm^2\,V^{-1}s^{-1}$). Measured mobilities are calibrated with respect to the reported experimental value for C_{60}^+ (4.321 $cm^2\,V^{-1}s^{-1}$; ref. 57).

species	K_0 (calc)	K_0 (meas)	meas/calc
C_{10}^+	9.80	10.00	1.02
$HC_{10}H^+$	8.04	8.20	1.02
C_{12}^+	8.44	8.55	1.01
$HC_{12}H^+$	6.96	7.13	1.02
C_{14}^+	7.34	7.46	1.01
$HC_{14}H^+$	6.17	6.27	1.02
C_{16}^+	6.47	6.59	1.02
$HC_{16}H^+$	5.52	5.62	1.02

also observe weak signals for hydrogenated carbon clusters, including the linear polyacetylene cations $HC_{2n}H^+$, which presumably arise from the reaction of carbon clusters formed in the laser ablation ion source with trace H_2O.

Table I summarizes measured reduced drift mobilities (K_0) for monocyclic carbon rings (C_n^+) and linear polyacetylene chains (HC_nH^+) over the n=10–16 range, derived from the measured arrival times adjusted for the time the ions spend in the hexapole and QMF, and calibrated with respect to the reported experimental value for C_{60}^+ (4.321 $cm^2\,V^{-1}s^{-1}$; ref. 57). To confirm assignment of the peaks to monocyclic carbon rings (C_n^+) and polyacetylene chains (HC_nH^+), reduced drift mobilities (K_0) for these structures were calculated using the IMoS 2.0 program suite[58] with the trajectory method parametrized for He buffer gas at T=298 K. Molecular geometries and input charge distributions were computed at the ωB97X-D/cc-pVTZ level of density functional theory, with the Merz-Singh-Kollman scheme parameterized to reproduce the electric dipole moments of the ions.[59] The calculated reduced mobilities agree well with the experimental values (Table I), supporting assignments of the ATD peaks to monocyclic carbon rings (C_n^+) and linear polyacetylene chains (HC_nH^+).

B. Electronic spectra of C_{14}^+ and $HC_{14}H^+$

As a first example of the IMS-MS-cryo instrument's capacity to spectroscopically characterize clusters with different masses and isomeric structures, we present data for the cyclic C_{14}^+ cluster and the linear $HC_{14}H^+$ polyacetylene cation. ATDs recorded with the QMF set to m/z 168 (corresponding to the major C_{14}^+ isotopologue) and m/z 170 (corresponding to the major $HC_{14}H^+$ isotopologue) are shown in Figure 3, where it can be seen that the linear HC_nH^+ polyacetylene molecules are ≈0.35 ms slower than the more compact cyclic C_{14}^+ clusters. Note, that a peak due to cyclic C_{14}^+ clusters containing two ^{13}C atoms or to a cyclic version of $HC_{14}H^+$ is apparent in the ATD obtained with the QMF tuned to m/z 170. The clear mobility separation of the C_{14}^+ clusters and the linear $HC_{14}H^+$ polyacetylene molecules makes it straightforward to select either species using the Bradbury-Nielsen gate at the end of the ion mobility drift region.

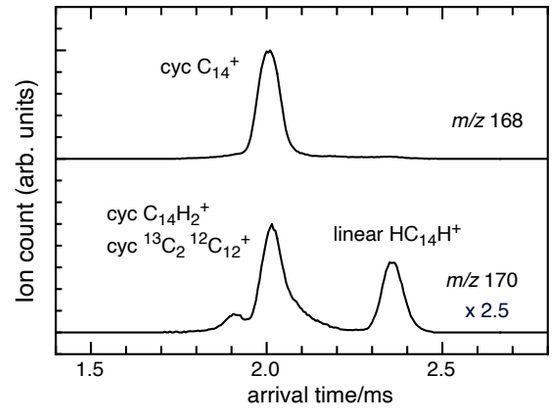

FIG. 3: ATDs for monocyclic C_{14}^+ (m/z 168) and linear $HC_{14}H^+$ (m/z 170) in He buffer gas. The C_{14}^+ peak in the m/z 170 ATD is presumably due to C_{14}^+ clusters containing two ^{13}C atoms, leakage of C_{14}^+ clusters containing one ^{13}C atom, and possibly cyclic $C_{14}H_2^+$ clusters.

The REPD spectra of $HC_{14}H^+$ and of C_{14}^+ selectively introduced into the cryogenically cooled QIT and tagged with N_2 are shown in Figure 4. The $HC_{14}H^+$-N_2 spectrum exhibits strong bands in the near infrared spectral range that correspond to bands previously reported

for the linear polyacetylene $HC_{14}H^+$ cation trapped in a Ne matrix.[60,61] In contrast, as previously reported,[62] the main electronic absorptions of the monocyclic C_{14}^+-N_2 cluster occur in the visible region (611.9 nm for the origin transition) with no discernible transitions in the infrared range.

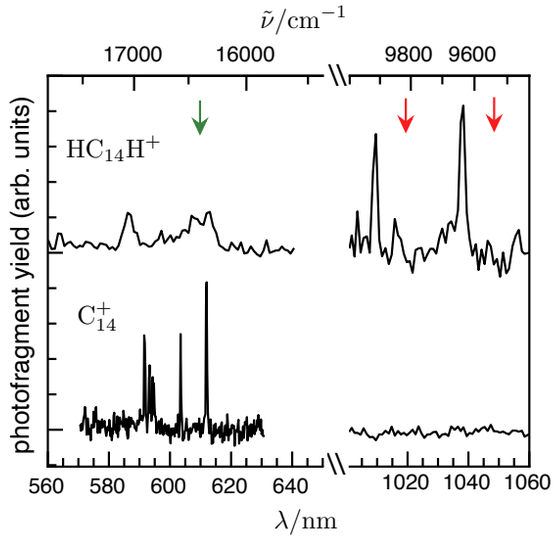

FIG. 4: REPD spectra of linear $HC_{14}H^+$-N_2 and monocyclic C_{14}^+-N_2. Red arrows indicate $\tilde{A}^2\Pi_g \leftarrow \tilde{X}^2\Pi_u$ absorptions of $HC_{14}H^+$ in a Ne matrix (1047.1 and 1019.5 nm from ref. 60), while the green arrow indicates a $\tilde{D}^2\Pi_g \leftarrow \tilde{X}^2\Pi_u$ absorption of $HC_{14}H^+$ in a Ne matrix (609.8 nm from ref. 61). Note the x-axis break.

C. Electronic spectra of monocyclic and bicyclic C_{28}^+

To demonstrate the IMS-MS-cryo instrument's capacity for obtaining electronic spectra of isomer-selected cluster ions we present data for C_{28}^+ clusters, which are known to have monocyclic and bicyclic isomers.[42,62] The ATD recorded with the QMF set to m/z 336 shown in Figure 5 exhibits peaks associated with monocyclic and bicyclic C_{28}^+ isomers, and a small fraction of multicharged C_{56}^{2+} and C_{84}^{3+} fullerenes. The slight asymmetry of the bicyclic isomer ATD peak is presumably due to the presence of isomers with the carbon atoms distributed between the two rings in different ways. The second and third traces show ATDs recorded when either the monocyclic isomer or bicyclic isomer(s) were mobility selected using the electrostatic Bradbury-Nielsen gate at the end of the drift region, demonstrating clean selection of either isomer.

REPD electronic spectra measured over the 710-1400 nm wavelength range for C_{28}^+ ions contained in the QIT and tagged with N_2 molecules are presented in Figure 6. Figures 6a&b show electronic spectra of C_{28}^+ without isomer selection, obtained at low and high laser power, respectively. In the low-power spectrum the peaks appear with their natural intensities, whereas weak spectral features are exaggerated in the high-power spectrum. Electronic spectra measured for mobility-selected C_{28}^+ monocyclic and bicyclic isomers are shown in Figures 6c&d, respectively. As reported previously,[62] the monocyclic C_{28}^+ spectrum is dominated by an origin transition at 7576 cm^{-1} ($\pm$20 cm^{-1}) and weaker transitions lying to shorter wavelength that are presumably due to in-plane ring deformation vibrational modes, with the peak at 9822 cm^{-1} (displaced from the origin by 2246 cm^{-1}) tentatively assigned to a C$\equiv$C stretch vibrational mode. The monocyclic C_{28}^+ spectrum (obtained at low laser power), resembles the low power spectrum measured with no gating (Figure 6a) indicating that the bicyclic isomer, despite having a comparable abundance to the monocyclic isomer, does not absorb significantly over this range. Indeed, it was necessary to expose the bicyclic C_{28}^+ isomer(s) with much higher laser powers to record the spectrum shown in Figure 6d. Without mobility selection the bicyclic C_{28}^+ isomer's weak features would be totally obscured by the stronger monocyclic absorptions apparent in Figure 6a–c. It is only when the bicyclic form is selectively introduced into the QIT that it is possible to record the electronic spectrum shown in Figure 6d. The bicyclic isomer spectrum does not possess a clear origin band or easily assignable vibronic peaks, although it is possible that other transitions lie outside the investigated spectral range (710-1400 nm). Furthermore, it is possible that several bicyclic isomers with similar CCSs, which are difficult to separate using the IMS, contribute to the spectrum.

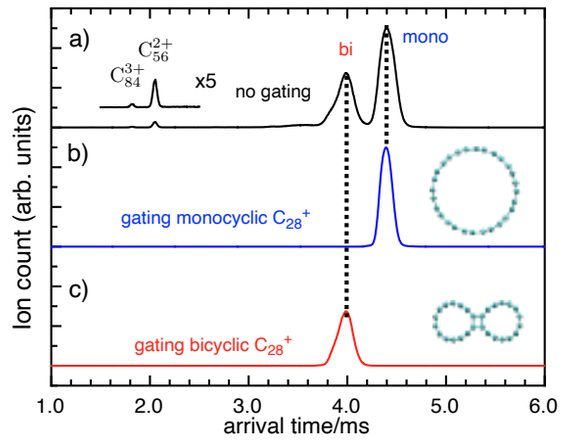

FIG. 5: (a) ATD for mass-selected C_{28}^+ clusters with the QMF set to m/z 336. (b) ATD for mobility-selected monocyclic C_{28}^+ clusters. (c) ATD for mobility-selected bicyclic C_{28}^+ clusters.

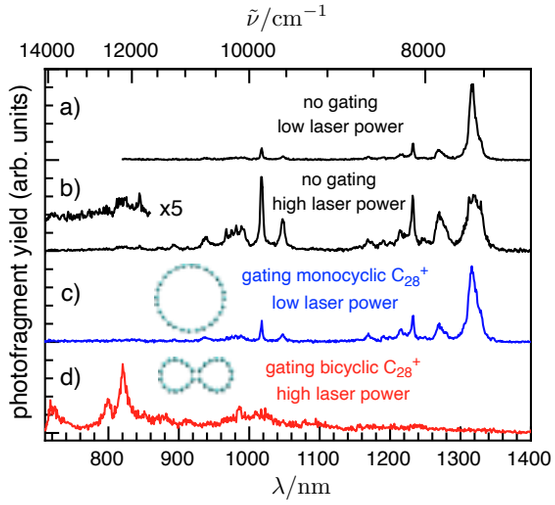

FIG. 6: (a) Electronic spectrum for C_{28}^+ clusters that were not isomer-selected (low laser power). (b) Electronic spectrum for C_{28}^+ clusters that were not isomer-selected (high laser power). (c) Electronic spectrum for isomer-selected monocyclic C_{28}^+ clusters (low laser power). (d) Electronic spectrum for isomer-selected bicyclic C_{28}^+ clusters (high laser power). Spectra were recorded by exposing C_{28}^+-$(N_2)_m$ complexes to tunable light in the QIT and monitoring C_{28}^+ photofragments.

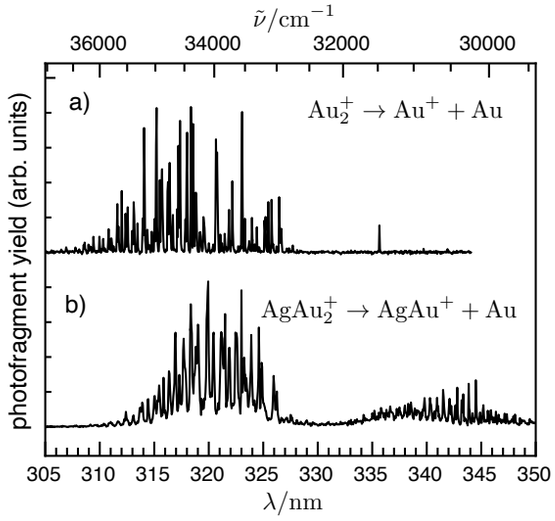

FIG. 7: (A) REPD electronic spectrum of Au_2^+ recorded by monitoring Au^+ photofragments as a function of wavelength. (b) REPD electronic spectrum of Au_2Ag^+ recorded by monitoring $AuAg^+$ photofragments as a function of wavelength.

D. Electronic spectra of Au_2^+ and Au_2Ag^+

To demonstrate the suitability of the instrument for spectroscopically probing metal clusters, we present the REPD spectra of Au_2^+ and Au_2Ag^+ over the 305–350 nm wavelength range (Figure 7), where the target cation clusters were created by laser ablation of a gold/silver alloy disk. The spectra were obtained with pure He buffer gas in the cryogenically cooled QIT. The Au_2^+ spectrum, which was obtained by monitoring the Au^+ photofragment yield as a function of wavelength, is similar to the spectrum reported in ref. 63, and exhibits a complex pattern of peaks with no clear vibronic progressions. The Au_2Ag^+ spectrum, which was recorded on the $AuAg^+$ photofragment channel, shows sharp spectral features across several band systems that correspond to broad, unresolved bands reported by Schäfer and co-workers.[64] Analysis of the Au_2Ag^+ spectrum is in progress. Although the isomer selectivity of the instrument is not required to study the metal dimers and trimers, larger gold and silver clusters, including Au_4^+,[65] are predicted to possess several isomers with similar energy,[66,67] and should be suitable spectroscopic targets for the instrument.

VI. SUMMARY AND OUTLOOK

The IMS-MS-cryotrap instrument provides a means for measuring electronic spectra of cooled, isomer-selected, charged molecules and clusters in the gas phase. The machine's capabilities have been demonstrated through several examples. First, it was shown that the cyclic C_{14}^+ carbon cluster and the linear $HC_{14}H^+$ polyacetylene cluster could be separated according to their masses and mobilities prior to spectroscopic interrogation in the cryogenic ion trap. Second, it was demonstrated that monocyclic and bicyclic isomers of C_{28}^+ could be cleanly separated, and that the two isomers have distinct REPD spectra. Without isomer separation prior to spectroscopic interrogation in the QIT, it would be extremely difficult to obtain the relatively weak spectrum of the bicyclic C_{28}^+ isomer over the 700-1200 nm range. As a final example, we showed that it was possible to generate the Au_2^+ dimer and Au_2Ag^+ trimer and measure their electronic transitions, demonstrating that metal clusters can be formed and spectroscopically interrogated with the instrument.

In future, the apparatus will be deployed for obtaining infrared and electronic spectra of diverse charged molecules and clusters composed of carbon, silicon, metal and hydrogen atoms, where the ability to select species according to both mass-to-charge ratio and collision cross section, should be useful for resolving ambiguities in assigning spectral features to particular isomers and for teasing out weak spectral features associated with minor isomers that may otherwise be obscured by stronger absorptions of more abundant isomers. It is also worth remarking that the laser ablation source should be suitable for producing a broad range of molecular ions through

matrix assisted laser desorption/ionization (MALDI). Finally, we note that although the performance of the instrument has been illustrated with cation clusters, reconfiguring for operation with anion clusters is straightforward and merely involves reversing the DC potentials applied to all electrodes.

ACKNOWLEDGMENTS

The authors thank Richard Mathys of the Science Faculty Workshop for exceptional contributions to the design and construction of the apparatus. This research was supported under the Australian Research Council's Discovery Project funding scheme (Project Numbers DP150101427 and DP160100474). J. T. B. acknowledges the University of Melbourne and Australian government for support through the Research Training Program (RTP) scholarship scheme.

DATA AVAILABILITY STATEMENT

The data that support the findings of this study are available from the corresponding author upon reasonable request.

[1]M. Okumura, L. I. Yeh, and Y. T. Lee, J. Chem. Phys. **88**, 79 (1988).
[2]D. W. Boo and Y. T. Lee, Int. J. Mass Spectrom. Ion Proc. **159**, 209 (1996).
[3]E. Bieske, A. Soliva, M. Welker, and J. Maier, J. Chem. Phys. **93**, 4477 (1990).
[4]M. A. Duncan, Int. J. Mass Spectrom. **200**, 545 (2000).
[5]E. J. Bieske and O. Dopfer, Chem. Rev. **100**, 3963 (2000).
[6]A. Dzhonson, D. Gerlich, E. Bieske, and J. Maier, J. Mol. Struct. **795**, 93 (2006).
[7]J. Jašík, J. Jábka, J. Roithová, and D. Gerlich, Int. J. Mass Spectrom. **354-355**, 204 (2013).
[8]J. A. Stearns, S. Mercier, C. Seaiby, M. Guidi, O. V. Boyarkin, and T. R. Rizzo, J. Am. Chem. Soc. **129**, 11814 (2007).
[9]T. R. Rizzo, J. A. Stearns, and O. V. Boyarkin, Int. Rev. Phys. Chem. **28**, 481 (2009).
[10]H. Kang, G. Féraud, C. Dedonder-Lardeux, and C. Jouvet, J. Phys. Chem. Lett. **5**, 2760 (2014).
[11]A. B. Wolk, C. M. Leavitt, E. Garand, and M. A. Johnson, Acc. Chem. Res. **47**, 202 (2014).
[12]Y. Inokuchi, R. Kusaka, T. Ebata, O. V. Boyarkin, and T. R. Rizzo, ChemPhysChem **14**, 649 (2013).
[13]S. Warnke, A. Ben Faleh, R. P. Pellegrinelli, N. Yalovenko, and T. R. Rizzo, Faraday Discuss. **217**, 114 (2019).
[14]S.-i. Ishiuchi, H. Wako, D. Kato, and M. Fujii, J. Mol. Spectrosc. **332**, 45 (2017).
[15]F. S. Menges, E. H. Perez, S. C. Edington, C. H. Duong, N. Yang, and M. A. Johnson, J. Am. Soc. Mass Spectrom. **30**, 1551 (2019).
[16]B. M. Marsh, J. M. Voss, and E. Garand, J. Chem. Phys. **143**, 204201 (2015).
[17]N. C. Polfer and J. Oomens, Mass Spectrom. Rev. **28**, 468 (2009).
[18]A. Günther, P. Nieto, D. Müller, A. Sheldrick, D. Gerlich, and O. Dopfer, J. Mol. Spec. **332**, 8 (2017).
[19]C. P. Harrilal, A. F. DeBlase, S. A. McLuckey, and T. S. Zwier, J. Phys. Chem. A **125**, 9394 (2021).
[20]O. Asvany and S. Schlemmer, Phys. Chem. Chem. Phys. **23**, 26602 (2021).
[21]S. Spieler, M. Kuhn, J. Postler, M. Simpson, R. Wester, P. Scheier, W. Ubachs, X. Bacalla, J. Bouwman, and H. Linnartz, Astrophys. J. **846**, 168 (2017).
[22]E. Mucha, A. I. González Flórez, M. Marianski, D. A. Thomas, W. Hoffmann, W. B. Struwe, H. S. Hahm, S. Gewinner, W. Schöllkopf, P. H. Seeberger, G. von Helden, and K. Pagel, Angew. Chem. Int. Ed. **56**, 11248 (2018).
[23]D. J. Goebbert, G. Meijer, and K. R. Asmis, AIP Conf. Proc. **1104**, 22 (2009).
[24]S. Chakrabarty, M. Holz, E. K. Campbell, A. Banerjee, D. Gerlich, and J. P. Maier, J. Phys. Chem. Lett. **4**, 4051 (2013).
[25]O. Dopfer, D. Roth, and J. P. Maier, Int. J. Mass Spectrom. **218**, 281 (2002).
[26]N. Solcà and O. Dopfer, J. Chem. Phys. **120**, 10470 (2004).
[27]K. Koyasu, T. Ohtaki, N. Hori, and F. Misaizu, Chem. Phys. Lett. **523**, 54 (2012).
[28]S. Warnke, C. Baldauf, M. T. Bowers, K. Pagel, and G. von Helden, J. Am. Chem. Soc. **136**, 10308 (2014).
[29]A. Masson, M. Z. Kamrath, M. A. S. Perez, M. S. Glover, U. Rothlisberger, D. E. Clemmer, and T. R. Rizzo, J. Am. Soc. Mass Spectrom. **26**, 1444 (2015).
[30]M. Z. Kamrath and T. R. Rizzo, Acc. Chem. Res. **51**, 1487 (2018).
[31]L. Voronina and T. R. Rizzo, Phys. Chem. Chem. Phys. **17**, 25828 (2015).
[32]B. Schindler, A. D. Depland, G. Renois-Predelus, G. Karras, B. Concina, G. Celep, J. Maurelli, V. Loriot, E. Constant, R. Bredy, C. Bordas, F. Lépine, and I. Compagnon, Int. J. Ion Mobil. Spectrom. **20**, 119 (2017).
[33]S. J. P. Marlton, B. I. McKinnon, B. Ucur, J. P. Bezzina, S. J. Blanksby, and A. J. Trevitt, J. Phys. Chem. Lett. **11**, 4226 (2020).
[34]O. Hernandez, S. Isenberg, V. Steinmetz, G. L. Glish, and P. Maitre, J. Phys. Chem. A **119**, 6057 (2015).
[35]N. J. A. Coughlan, W. Fu, M. Guna, B. B. Schneider, J. C. Y. Le Blanc, J. L. Campbell, and W. S. Hopkins, Phys. Chem. Chem. Phys. **23**, 20607 (2021).
[36]S. Warnke, A. B. Faleh, R. P. Pellegrinelli, N. Yalovenko, and T. R. Rizzo, Faraday Discuss. **217**, 114 (2019).
[37]A. B. Faleh, S. Warnke, and T. R. Rizzo, Anal. Chem. **91**, 4876 (2019).
[38]B. D. Adamson, N. J. A. Coughlan, P. B. Markworth, R. E. Continetti, and E. J. Bieske, Rev. Sci. Instrum. **85**, 123109 (2014).
[39]A.-L. Simon, F. Chirot, C. M. Choi, C. Clavier, M. Barbaire, J. Maurelli, X. Dagany, L. MacAleese, and P. Dugourd, Rev. Sci. Instrum. **86**, 094101 (2015).
[40]R. Fromherz, G. Ganteför, and A. A. Shvartsburg, Phys. Rev. Lett. **89**, 083001 (2002).
[41]M. Vonderach, O. T. Ehrler, P. Weis, and M. M. Kappes, Anal. Chem. **83**, 1108 (2011).
[42]G. von Helden, M. T. Hsu, N. Gotts, and M. T. Bowers, J. Phys. Chem. **97**, 8182 (1993).
[43]N. G. Gotts, G. von Helden, and M. T. Bowers, Int. J. Mass Spectrom. Ion Proc. **149-150**, 217 (1995).
[44]M. F. Jarrold and J. E. Bower, J. Chem. Phys. **96**, 9180 (1992).
[45]R. R. Hudgins, M. Imai, M. F. Jarrold, and P. Dugourd, J. Chem. Phys. **111**, 7865 (1999).
[46]P. Weis, T. Bierweiler, S. Gilb, and M. M. Kappes, Chem. Phys. Lett. **355**, 355 (2002).
[47]S. Gilb, P. Weis, F. Furche, R. Ahlrichs, and M. M. Kappes, J. Chem. Phys. **116**, 4094 (2002).
[48]F. Furche, R. Ahlrichs, P. Weis, C. Jacob, S. Gilb, T. Bierweiler, and M. M. Kappes, J. Chem. Phys. **117**, 6982 (2002).
[49]P. Weis, O. Welz, E. Vollmer, and M. M. Kappes, J. Chem. Phys. **120**, 677 (2004).
[50]J. W. J. Wu, R. Moriyama, M. Nakano, K. Ohshimo, and F. Misaizu, Phys. Chem. Chem. Phys. **19**, 24903 (2017).
[51]K. Ohshimo, T. Komukai, R. Moriyama, and F. Misaizu, J. Phys. Chem. A **118**, 3899 (2014).

[52]E. K. Campbell and P. W. Dunk, Rev. Sci. Instrum. **90**, 103101 (2019).
[53]H. E. Revercomb and E. A. Mason, Anal. Chem. **47**, 970 (1975).
[54]K. Kaplan, S. Graf, C. Tanner, M. Gonin, K. Fuhrer, R. Knochenmuss, P. Dwivedi, and H. H. Hill, Anal. Chem. **82**, 9336 (2010).
[55]N. E. Bradbury and R. A. Nielsen, Phys. Rev. **49**, 388 (1936).
[56]X.-B. Wang and L.-S. Wang, Rev. Sci. Instrum. **79**, 073108 (2008).
[57]P. Dugourd, R. R. Hudgins, D. E. Clemmer, and M. F. Jarrold, Rev. Sci. Instrum. **68**, 1122 (1997).
[58]V. Shrivastav, M. Nahin, C. J. Hogan, and C. Larriba-Andaluz, J. Am. Soc. Mass Spectrom. **28**, 1540 (2017).
[59]B. H. Besler, K. M. Merz Jr., and P. A. Kollman, J. Comput. Chem. **11**, 431 (1990).
[60]P. Freivogel, J. Fulara, D. Lessen, D. Forney, and J. Maier, Chem. Phys. **189**, 335 (1994).
[61]J. Fulara, M. Grutter, and J. P. Maier, J. Phys. Chem. A **111**, 11831 (2007).
[62]J. T. Buntine, M. I. Cotter, U. Jacovella, C. Liu, P. Watkins, E. Carrascosa, J. N. Bull, L. Weston, G. Muller, M. Scholz, and E. Bieske, J. Chem. Phys. **155**, 214302 (2021).
[63]M. Förstel, K. M. Pollow, K. Saroukh, E. A. Najib, R. Mitric, and O. Dopfer, Angew. Chem. Int. Ed. **59**, 21403 (2020).
[64]A. Shayeghi, L. F. Pašteka, D. A. Götz, P. Schwerdtfeger, and R. Schäfer, Phys. Chem. Chem. Phys. **20**, 9108 (2018).
[65]M. Förstel, W. Schewe, and O. Dopfer, Angew. Chem. Int. Ed. **131**, 3394 (2019).
[66]A. Shayeghi, D. A. Götz, R. L. Johnston, and R. Schäfer, Eur. Phys. J. D **69**, 152 (2015).
[67]A. Shayeghi, R. L. Johnston, and R. Schäfer, J. Chem. Phys. **141**, 181104 (2014).

(a)

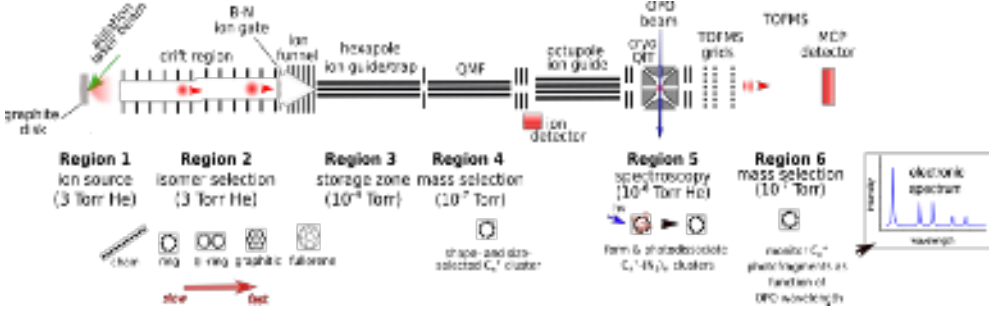
ablation laser
B-N ion gate
drift region
ion funnel
hexapole ion guide/trap
QMF
octupole ion guide
cryo QIT
OPO beam
TOFMS
TOFMS grids
MCP detector
graphite disk
ion detector
Region 1
ion source
(3 Torr He)
Region 2
isomer selection
(3 Torr He)
Region 3
storage zone
(10⁻⁴ Torr)
Region 4
mass selection
(10⁻⁷ Torr)
Region 5
spectroscopy
(10⁻⁴ Torr He)
Region 6
(10⁻⁷ Torr)
electronic spectrum
wavelength
slow
fast

(b)

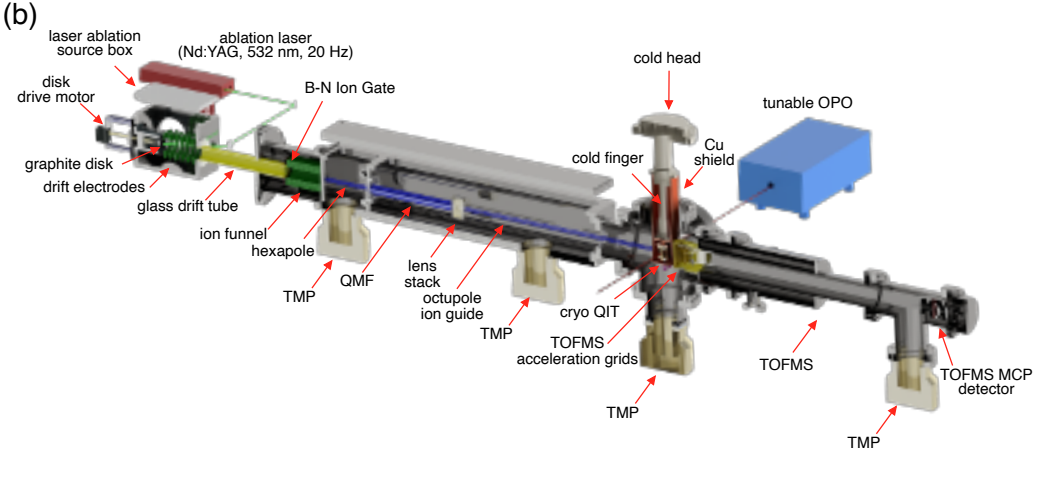
laser ablation source box
ablation laser (Nd:YAG, 532 nm, 20 Hz)
disk drive motor
B-N Ion Gate
cold head
tunable OPO
graphite disk
drift electrodes
glass drift tube
cold finger
Cu shield
ion funnel
hexapole
TMP
QMF
lens stack
octupole ion guide
TMP
cryo QIT
TOFMS acceleration grids
TMP
TOFMS
TOFMS MCP detector
TMP

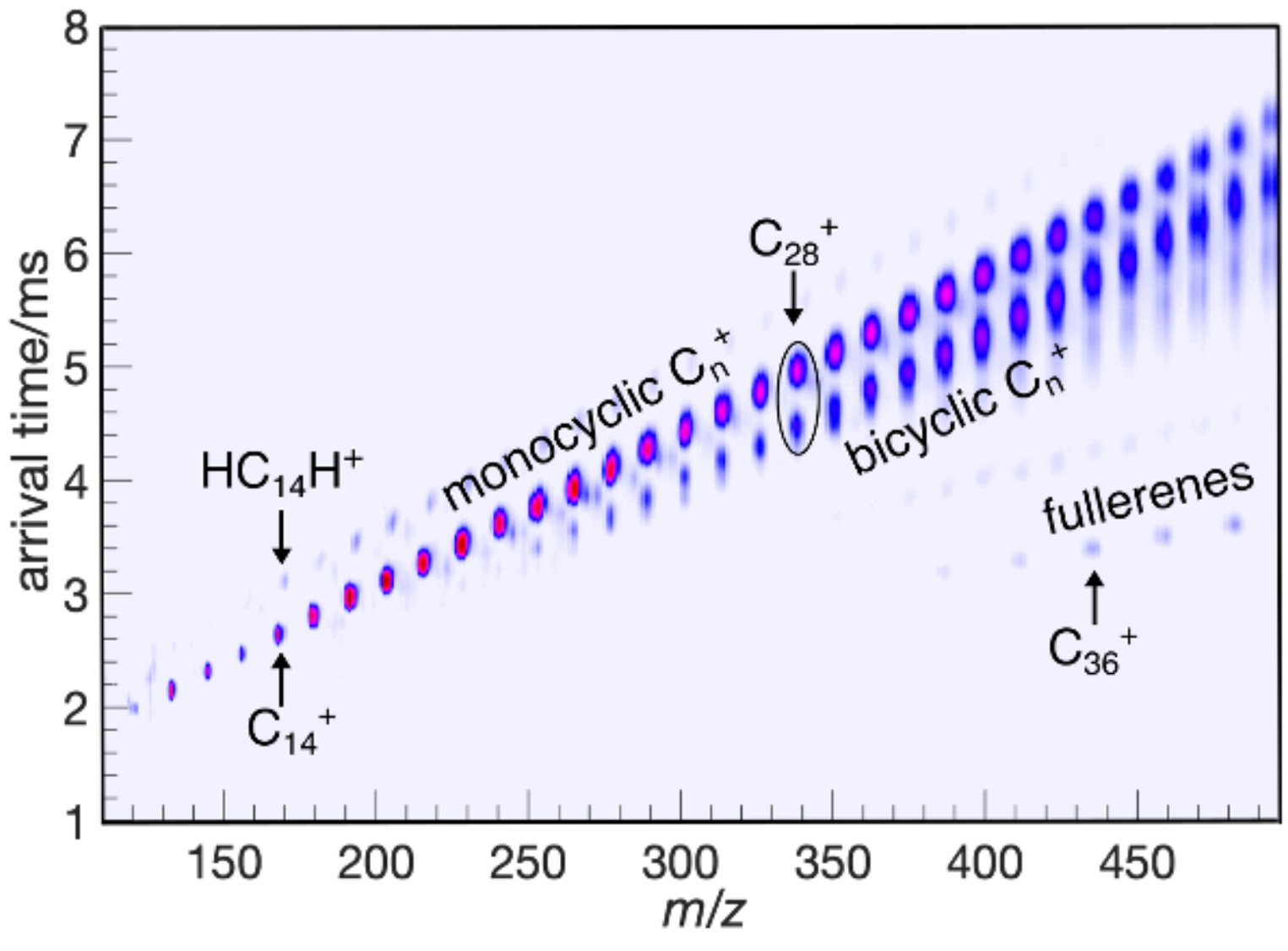
arrival time/ms
m/z
HC14H+
C14+
monocyclic Cn+
C28+
bicyclic Cn+
fullerenes
C36+

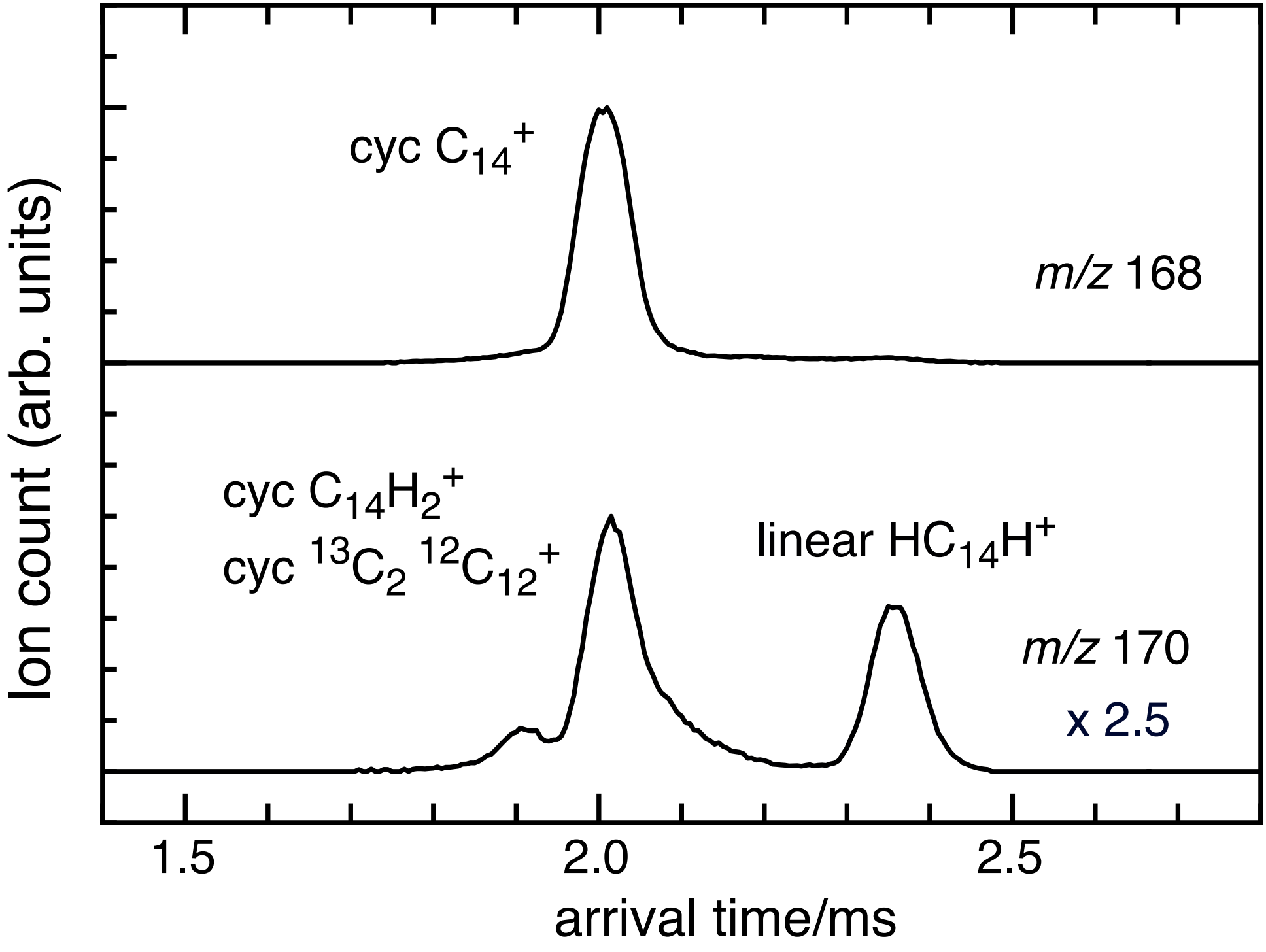
cyc C_{14}^+
m/z 168
cyc $C_{14}H_2^+$
cyc $^{13}C_2\,^{12}C_{12}^+$
linear $HC_{14}H^+$
m/z 170
x 2.5
Ion count (arb. units)
1.5
2.0
2.5
arrival time/ms

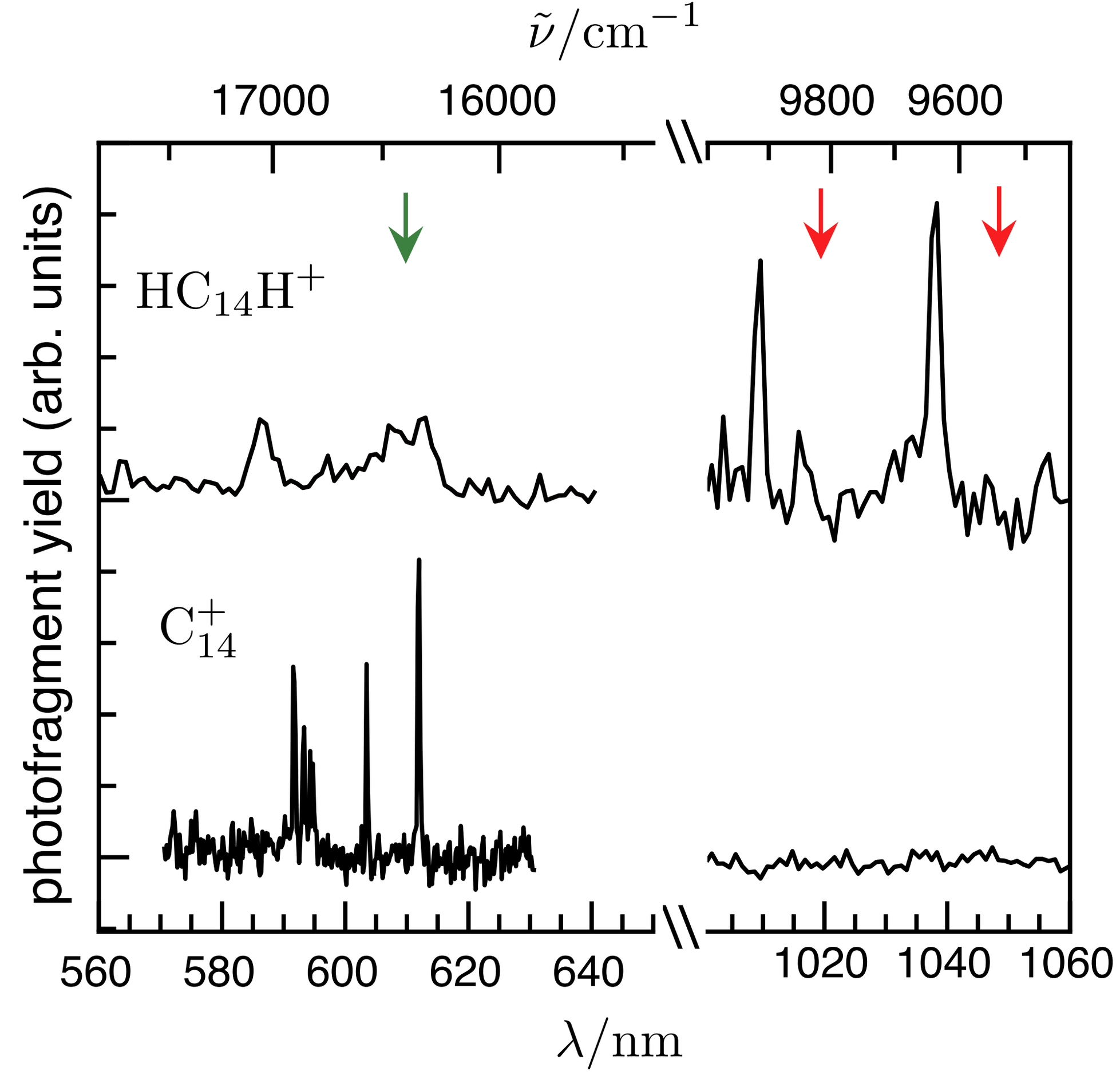
$\tilde{\nu}/\mathrm{cm}^{-1}$
17000
16000
9800
9600
$HC_{14}H^+$
C_{14}^+
photofragment yield (arb. units)
560
580
600
620
640
1020
1040
1060
λ/nm

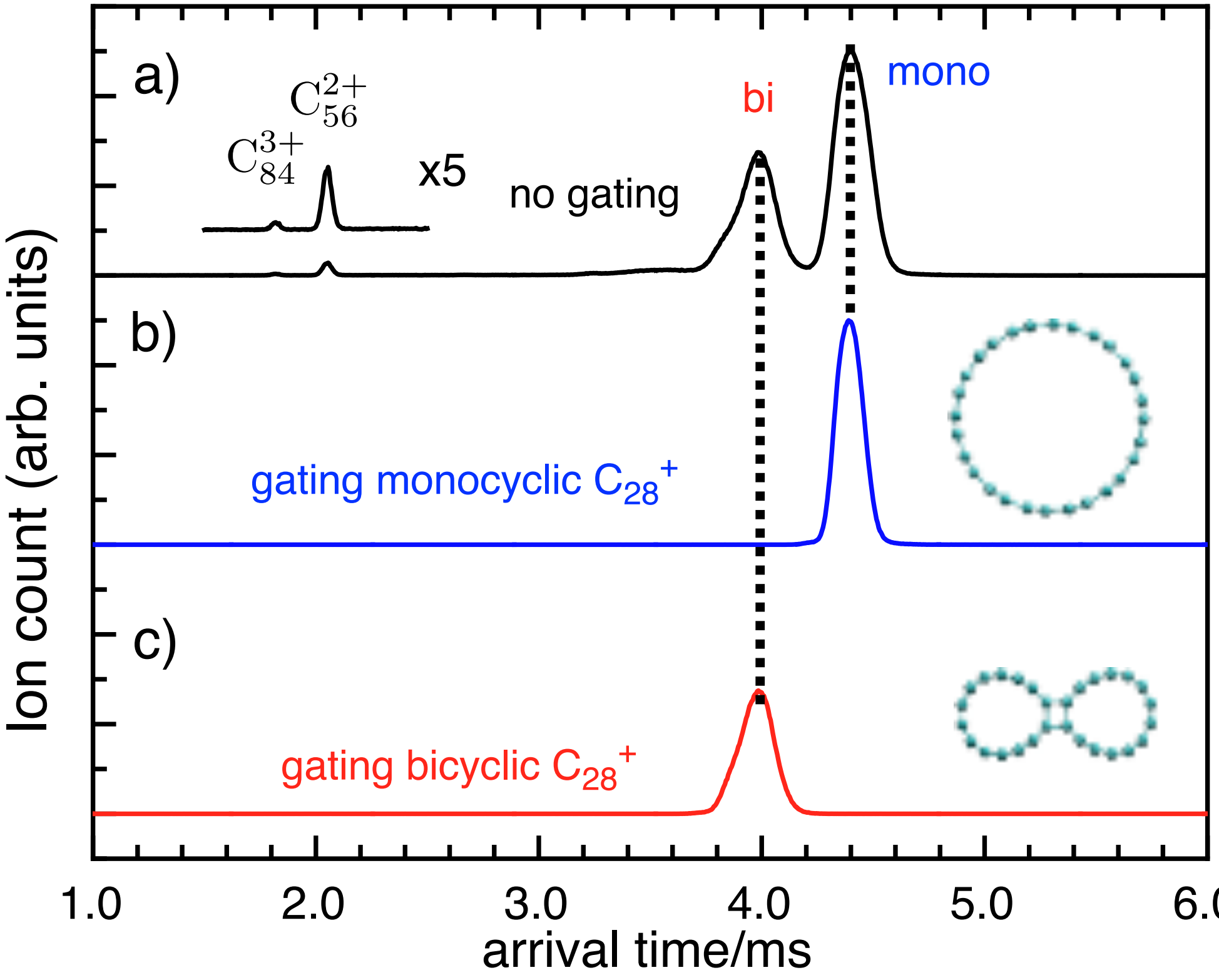
a)
C_{56}^{2+}
C_{84}^{3+}
x5
no gating
bi
mono
b)
gating monocyclic C_{28}^{+}
c)
gating bicyclic C_{28}^{+}
Ion count (arb. units)
1.0
2.0
3.0
4.0
5.0
6.0
arrival time/ms

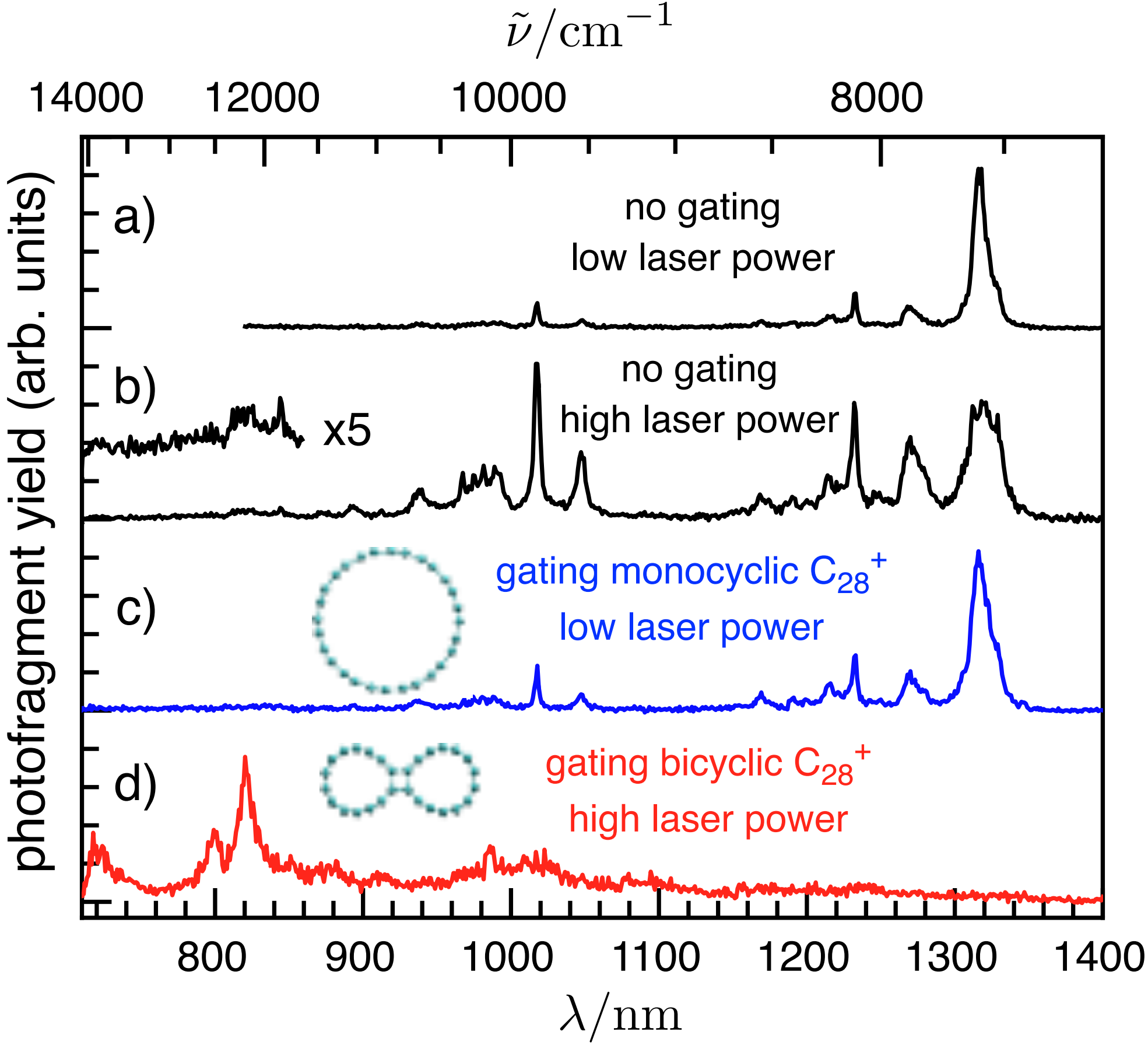
$\tilde{\nu}/\mathrm{cm}^{-1}$
14000
12000
10000
8000
a)
no gating
low laser power
b)
x5
no gating
high laser power
c)
gating monocyclic C_{28}^+
low laser power
d)
gating bicyclic C_{28}^+
high laser power
photofragment yield (arb. units)
800
900
1000
1100
1200
1300
1400
λ/nm

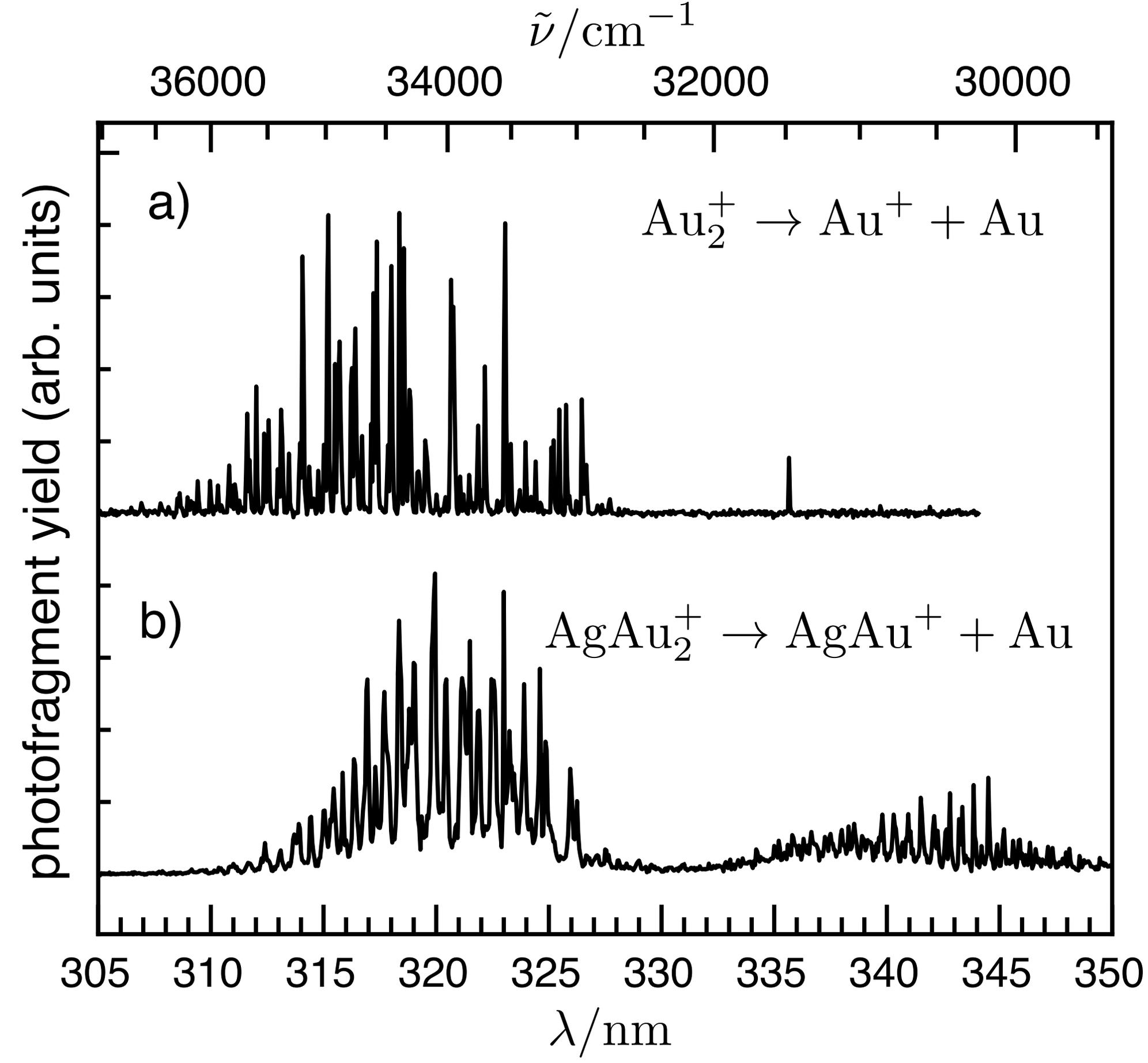
$\tilde{\nu}/\mathrm{cm}^{-1}$
36000
34000
32000
30000
a)
$\mathrm{Au}_2^+ \rightarrow \mathrm{Au}^+ + \mathrm{Au}$
b)
$\mathrm{AgAu}_2^+ \rightarrow \mathrm{AgAu}^+ + \mathrm{Au}$
photofragment yield (arb. units)
305
310
315
320
325
330
335
340
345
350
λ/nm